

## Looking for an extra dimension with tomographic cosmological shear

Yong-Seon Song

Enrico Fermi Institute, University of Chicago, Chicago IL 60637

(Dated: March 20, 2024)

The cosmological acceleration was discovered in one of the brane-based models. We are interested in discriminating this model from the dark energy by tomographic cosmological shear. Growth factors are different in the two models when one adjusts parameters to get nearly identical  $H(z)$ . The two models could be distinguished with independent determinations of both geometrical factors and the growth factor. We introduce new parameterizations to separate the influence of geometry and the influence of growth on cosmological shear maps. We find that future observations will be able to distinguish between both models.

PACS numbers: draft

## I. INTRODUCTION

The discovery of cosmological acceleration [1, 2, 3] has led to theoretical efforts to understand the nature of the cosmological acceleration [4, 5, 6, 7] and phenomenological efforts to discriminate the diverse modelings [8, 9, 10, 11, 12, 13, 14]. Most theoretical explanations for the acceleration preserve Einstein gravity and add a new smooth and dark component called Dark Energy (DE) [4, 5]. However, DE is not yet strongly supported theoretically nor phenomenologically. The similar cosmological acceleration was also discovered in one of brane-based models [6] by C. Dey et al. [15, 16] (hereafter DGP model represents this discovery of the cosmological acceleration in the brane-based model [6].)

In the DGP model, the cosmological acceleration is generated by the modified gravity due to the presence of the extra dimension in DGP. The study of the extra dimension physics in unifying the DGP model has been investigated by [17, 18, 19]. Dvali, Gabadadze and Porrati designed a brane where ordinary matter is embedded in an infinite extra dimension and gravity is modified at larger scale [6]. The model (DGP) which generates the cosmological acceleration based upon [6]-type braneworld was proposed in [15, 16].

While the DE growth factor is suppressed by dark energy component domination over matter component, the DGP growth factor is suppressed by the weakened gravity. We derive the DGP growth factor by using the set of continuity equations of ordinary matter confined to the DGP brane. We find that the DGP growth factor departs noticeably from the DE growth factor even with nearly identical expansion rate  $H(z)$ . A slight difference is noticed from previous work based upon a different idea [20].

The constraints from cosmological shear maps on DE with a model-dependent parameterization have been studied in [13, 21, 22, 23, 24, 25, 26]. The cosmological parameters related to DE are determined by a distinct evolution of a

geometrical factor and a growth factor. We introduce a more general parameterization to determine directly, from cosmological shear data, the distance and the growth factor as a function of redshift. Both quantities can be precisely determined by the combination of the future CMB experiments and the future cosmological shear surveys. We investigate how to probe the difference between the DGP growth factor and the DE growth factor with  $H(z)$  determined through its geometrical influence on shear data.

## II. DGP MODEL

We briefly review the DGP model and set up a formalism to draw our result. We consider a  $(4+1)$ -dimensional model in which no energy sources are present at an infinite bulk dimension except at a  $(3+1)$ -dimensional brane embedded in the bulk. The Einstein-Hilbert action is

$$S_{(5)} = \frac{M_{(5)}^3}{16} \int d^5x \sqrt{-g_{(5)}} R_{(5)}; \quad (1)$$

where the subscript (5) denotes that quantities are five-dimensional, and  $M_{(5)}$  is the Planck mass in  $(4+1)$ -dimension. We add a  $(3+1)$ -dimensional brane with matter fields and the induced metric to the action Eq. 1. The embedded three-brane action is [6]

$$S_{(4)} = \int d^4x \sqrt{-g_{(4)}} \left[ -\frac{1}{2} L_m - \frac{M_{(4)}^2}{16} R_{(4)} \right]; \quad (2)$$

where the subscript (4) denotes that quantities are four-dimensional, and  $M_{(4)}$  is the Planck mass in  $(3+1)$ -dimension.

We introduce a five-dimensional metric with a line element

$$ds_{(5)}^2 = -dt^2 + a^2(t; y)_{ij} dx^i dx^j + dy^2; \quad (3)$$

where a flat metric is used for spatial dimensions and the coordinate  $y$  represents the extra dimension. Our universe is located at hypersurface  $y = 0$  where a lapse function is given by  $n(t; 0) = 1$  and a spatial expansion

---

Electronic address: ysong@cfp.uchicago.edu

factor  $a(t;0)$  is determined by the cosmic expansion of our universe [15].

In the DGP model, the gravitational force at short distances smaller than the crossover length  $r_c$  scales as  $1/r^2$  and the gravitational force at large distances bigger than  $r_c$  scales as  $1/r^3$ . The crossover length scale  $r_c$  is given by

$$r_c = \frac{M_{(4)}^2}{2M_{(5)}^3} : \quad (4)$$

When the Hubble horizon  $H^{-1}$  is close to  $r_c$ , the gravity is weakened and the cosmic expansion is accelerated. It is an alternative explanation of the cosmic acceleration with the absence of a dark energy component. We investigate the phenomenological consequences of a DGP-type extra dimension in the following subsections, such as the geometrical factor and the growth factor.

#### A . The geometrical factor of DGP

The Einstein equations from Eq. 1 and Eq. 2 are

$$G_{(5)B}^A - R_{(5)B}^A - \frac{1}{2}Rg_{(5)B}^A = \frac{8}{M_{(5)}^3}T_{(5)B}^A : \quad (5)$$

The tensor  $T_{(5)B}^A$  is composed of the energy momentum tensors of the bulk and the brane and the scalar curvature of the induced metric introduced in Eq. 2. We assume that the bulk is empty and the brane has only pressureless matter components. Then the total energy is

$$\rho_m = \frac{3M_{(4)}^2}{8} \left( \frac{\dot{a}}{a} \right)^2 : \quad (6)$$

The first term of right side of Eq. 6 is the matter density confined to the brane and the second term comes from the scalar curvature of the brane [15].

By considering the first integral of Eq. 5 and the proper junction condition defining the derivative of  $a(t;y)$  in terms of  $y$  at crossing the surface  $y = 0$ , we get the following brane-FLRW equation

$$H^2 + \frac{H}{r_c} = \frac{8}{3M_{(4)}^2} \rho_m ; \quad (7)$$

where  $\epsilon$  denotes signature  $(+, -)$ . To be consistent with the observed cosmic acceleration, we choose the negative sign for  $\epsilon$ . The negative sign implies de Sitter-like brane embedding in the extra dimension. The effect of the gravity leaking into the extra dimension is significant at  $H^{-1} = r_c$  but is negligible at  $H^{-1} \ll r_c$  [15, 16].

From Eq. 7 we get

$$H(a) = H_0 \left[ \frac{r_c}{a} + \frac{1}{2} \left( \frac{r_c}{a} \right)^2 \right]^{1/2} ; \quad (8)$$

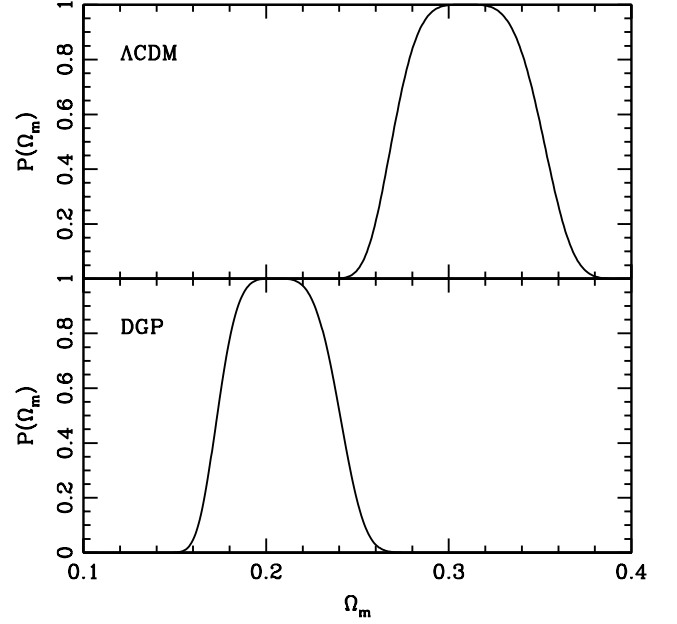


FIG. 1: Probability distribution of  $\Omega_m$  by the supernova data: top panel shows the fit of  $\Lambda$ CDM and the bottom panel shows the fit of DGP.

where the constant  $c$  is  $c = (1 - 2r_c H_0)^2$ . The flatness constraint is imposed to relate  $c$  to  $\Omega_m$  as  $c = [(1 - \Omega_m)/2]^2$ . Accordingly the crossover length scale is always greater than the present Hubble horizon to avoid the negative value of  $\rho_m$  or the empty universe ( $r_c > H^{-1}$ ). There have already been attempts to fit the supernova data with DGP [27, 28, 29]. We use the 'golden set' of supernova measurements [30] and compare the likelihood function of  $\Lambda$ CDM model with DGP. There is only a slight difference in the minimum  $\chi^2$  between  $\Lambda$ CDM and DGP,  $\chi_{\min}^2 = 178$  for  $\Lambda$ CDM and  $\chi_{\min}^2 = 179$  for DGP. As far as the supernova experiment is concerned, both models are almost equally probable.  $\Lambda$ CDM model prefers high  $\Omega_m$  around 0.3 and DGP prefers low  $\Omega_m$  around 0.2 (Fig. 1).

#### B . The growth factor of DGP

We choose the Gaussian normal longitudinal (GNL) gauge to fix the degrees of gauge freedom in 5D gravity. In GNL gauge, the extra dimension is not perturbed and any transition of energy from the extra dimension to time coordinate or spatial coordinates is not allowed. Then we have the usual  $(3+1)$ -dimensional longitudinal gauge on the brane which leads to the perturbations in the time and spatial coordinates as

$$\begin{aligned} g_{00} &= -1 - 2\phi(t; \mathbf{x}; y=0); \\ g_{ij} &= a^2(t; y=0) [1 + 2\psi(t; \mathbf{x}; y=0)] \delta_{ij} : \end{aligned} \quad (9)$$

The 00 component of perturbed Einstein equation is given by [31, 32]

$$\frac{2}{a^2} \dot{h} k^2 + 3\ddot{a} - \dot{a}^2 = \frac{1}{6} \frac{8}{M_{(5)}^3} ; \quad (10)$$

where  $\dot{h}$  is given by Eq. 6 and  $\ddot{a}$  is given by

$$= m \frac{8}{3M_{(4)}^2} \frac{2}{a^2} \dot{h} k^2 + 3\ddot{a} - \dot{a}^2 : \quad (11)$$

Neglecting the contribution of velocity perturbations, we write the Poisson equation by using Eq. 6, Eq. 10 and Eq. 11 as

$$k^2 = \frac{4}{M_{(4)}^2} a^2 m \frac{1}{1 - \frac{1}{2r_c H}} m ; \quad (12)$$

where  $m$  denotes the density contrast  $m = \delta$ . We do not consider  $m = 1$  case which is ruled out by the current measure distance.

The presence of Weyl component [32] does not deform the Poisson equation Eq. 12. The contribution of Weyl component is linearly added to the matter component with suppression factor of  $1=2r_c H$  at early time. It could be important at later time when  $1=2r_c H$  is close to unity. But in GN coordinate gauge, the trace of Weyl component vanishes and the fluid behaves like the radiation component. If Weyl fluid behaves like the radiation component then the clustering of that component is suppressed and eventually it guarantees the approximation of smallness of Weyl contribution against the matter clustering.

In the DGP model, matter does not flow into the extra dimension, i.e. there is no momentum component along the extra dimension  $y$ . The perturbation length scales of interest in this paper range approximately from  $10^4 H_0^{-1}$  to  $10^3 H_0^{-1}$ . In this range, the gravity of density fluctuations is not dissipated into the extra dimension significantly since the physical scales of those modes are much greater than  $1=r_c$ . Despite the presence of the extra dimension the set of coupled continuity equations of matter is not altered. In those intermediate scales, the coupled equations are

$$\begin{aligned} \frac{d\delta_m}{d} + ikv_m &= 0; \\ \frac{dv_m}{d} + aH v_m &= ik ; \end{aligned} \quad (13)$$

where we differentiate the matter perturbation  $\delta_m$  and the velocity perturbation  $v_m$  in terms of the comoving time  $d$ .

Second order differential equation from Eq. 13 can be written as

$$\frac{d^2}{d^2} + aH \frac{d}{d} k^2 = 0; \quad (14)$$

By using Eq. 7 and Eq. 12, the curvature perturbation is given by the background expansion rate  $H(z)$  as

$$k^2 = \frac{3}{2} a^2 H^2 \frac{1}{1 - \frac{1}{2r_c H}} m ; \quad (15)$$

The curvature perturbation of DE is suppressed by the ratio of matter component to the gross energy in the universe, but the curvature perturbation of DGP is suppressed by the weakened gravity. The difference in causes of suppression leads to the distinct evolution of growth factors of DE and DGP.

### III. MODEL INDEPENDENT PARAMETRIZATION

In this section we introduce a new parametrization to measure directly the geometrical factor and the growth factor by tomographic cosmic shear. First, we briefly discuss cosmic shear.

The size and shape of galaxies is altered by gravitational lensing. The effect of lensing is described by the convergence measuring the magnification or demagnification and the shear components,  $\gamma_1$  and  $\gamma_2$ , quantifying the distortion of shape [33, 34]. The shear components can be inferred from measurement of galaxy ellipticities which are composed of an intrinsic ellipticity and a lensing-induced ellipticity. In the absence of correlations between the intrinsic ellipticities, the rms error in the measurement of each shear component is

$$(\gamma_1) = (\gamma_2) = \frac{\gamma_{rms}}{N_{pix}} ; \quad (16)$$

where  $\gamma_{rms}$  is the rms intrinsic shear of the galaxies and  $N_{pix}$  is the number of galaxies in the pixel.

We assume that photometrically-determined redshifts can be used to sort the source galaxies into eight redshift bins with  $z = 0.4$  from  $z = 0.0$  to  $z = 3.2$  [21]. Maps of the shear components can be decomposed into even parity E modes and odd parity B modes. The signal contribution to the covariance of shear E modes is correlated across bins, but otherwise diagonal. The E modes shear,  $\gamma_E$ , power spectra are

$$C_{lij}^{EE} = \frac{1}{2} \int dr r W(r_i; r) W(r_j; r)^2 (k_z; r); \quad (17)$$

where  $r_i$  denotes the angular diameter distance to the median redshift of bin  $i$ . The geometrical factor appears in the window function  $W$  and the growth factor appears in dimensionless curvature power spectrum  $\delta^2$ . We show how to measure directly those quantities in the following subsections.

#### A. Parametrization of the angular diameter distance

The lensing-induced ellipticities are weighted by the mean location of sources in the window function  $W(r; r)$

Experiment	$l_{\text{max}}^T$	$l_{\text{max}}^{EB}$	(GHz)	$b$	$T$	$P$
Planck	2000	2500	100	9.2'	5.5	1
			143	7.1'	6	11
			217	5.0'	13	27
CM B pol	2000	2500	217	3.0'	1	1.4

TABLE I: The specifications of CM B experiments

given by

$$W(r_i; r) = \frac{r_i}{r_i r} \quad (\text{for } r < r_i; 0 \text{ otherwise}): \quad (18)$$

We directly parametrize the geometrical factor  $r_i$  instead of determining  $r_i$  by the cosmological parameters depending on the model choice between DGP and DE.

#### B. Parametrization of the growth factor

The dimensionless curvature power spectrum in Eq. 17 is

$$\Delta^2(k; r(z)) = \frac{2}{k^3} A_0 g(z)^2 T(k; z)^2; \quad (19)$$

where  $A_0$  is the primordial amplitude,  $g(z)$  is growth function of and  $T(k; z)$  is the transfer function. Here we are interested in the intermediate scales from  $10^4 H_0^{-1}$  to  $10^3 H_0^{-1}$  where the perturbations of the dark energy do not grow significantly to influence on the matter perturbations in DE, and the gravity of perturbations does not dissipate into the extra dimension in DGP. In those scales, the transfer function with negligible time dependence can be determined without the detailed knowledge of DE or DGP, and the departure from the linearity of density perturbations is not significant.

We parametrize the growth factor by discretizing its evolution in each  $z$  bin as

$$F_i = A_0 \frac{g(z_i)^2}{a^2}; \quad (20)$$

where the growth factor  $F_i$  of matter perturbations is averaged inside each bin  $i$  and is normalized to  $A_0$  in the matter dominated era. The curvature growth factor  $g$  is related to the matter perturbation growth factor  $g$  by Eq. 12.

## IV. EXPERIMENTS AND RESULTS

We sort out the cosmological parameters into three groups: primordial parameters, intermediate parameters and low redshift parameters. The primordial parameters come from a generic parametrization of structureless initial conditions. The intermediate parameters contribute

Experiment	$f_{\text{sky}}$	$n_{\text{tot}}$	$n_{\text{tot}} = \frac{2}{m_s}$
G2	0.5	65	1900
S3000	0.072	100	2920

TABLE II: Weak lensing experimental parameters assumed. Units for the total source sky density  $n_{\text{tot}}$  is  $1/\text{arcmin}^2$  and the per-component  $m_s$  shear  $m_s$  is evaluated at  $z = 1$ .

to leave a signature on CM B acoustic peaks at last scattering surface. The low redshift parameters affect the density fluctuations at later times. The primordial parameters consist of the primordial scalar amplitude  $A_0$ , the scalar spectral index  $n_s$  and the scalar running of the spectral index  $r_s$ . The intermediate parameters consist of the matter component  $\Omega_m$ , the baryon component  $\Omega_b$ , the helium fraction  $y_{\text{He}}$  and the angular extent of sound horizon at the last scattering surface  $\theta_s$ . The low redshift parameters consist of the neutrino mass  $m_\nu$ , the reionization redshift  $z_{\text{re}}$  and all other parameters related to the cosmic acceleration.

We consider the combination of CM B experiment with weak lensing survey in order to simultaneously constrain all cosmological parameters. The CM B angular power spectrum leads to tight constraints on the primordial parameters and intermediate parameters. The power of constraints on all cosmological parameters with CM B alone is shown in [35], and the constraints on the cosmological parameters by the combination of CM B and weak lensing are extensively studied in [13, 25]. The primordial parameters and intermediate parameters are tightly constrained with the future CM B experiments (see specifications in TABLE I).

The primordial amplitude  $A_0$  can be precisely determined by CM B alone [35]. The overall amplitude shift of CM B power spectra also results from the scattering of photons by ionized gas in the intergalactic medium. Though both cosmological parameters  $A_0$  and  $z_{\text{re}}$  are degenerate in most scales, the degeneracy between  $A_0$  and  $z_{\text{re}}$  is broken by the reionization bump of CM B polarization anisotropies in large scales. But the precision is limited by the unknown reionization history [36]. The primordial scalar amplitude  $A_0$  can be determined up to 1.7 percent level of accuracy in the absence of lensing contribution.

For the future weak lensing surveys, we assume uniform coverage which gives a diagonal noise covariance matrix  $N$ ,

$$N_{lm\ i; l'm'\ j} = \frac{2}{n_i} \frac{m_s}{m_s} \delta_{ll'} \delta_{mm'} \delta_{ij} \quad (21)$$

where  $n_i$  is the number of source galaxies per pixel in the given bin  $i$ . We use a ground-based survey G2, and a space-based surveys S3000. The specifications for those surveys are shown in TABLE II. The advantages of space are not fully exploited in this analysis which is only using

information on large-scale. The galaxy number distribution for the ground-based survey G2 are inferred from observations with the Subaru telescope [37]. The analytic expression for this distribution is well matched with

$$\begin{aligned} dn=dz & \quad z^{1.3} \exp(-z/1.2)^{1.2} & (z < 1) \\ dn=dz & \quad z^{1.1} \exp(-z/1.2)^{1.2} & (z > 1) \end{aligned} \quad (22)$$

We normalize the total number of galaxies  $n_{\text{tot}}$  as 65 per square arcmin after reducing  $dn=dz$  a half in the  $1.2 < z < 2.5$  due to inaccurate photometric redshift observation [38]. For the space-based survey, the distribution function is

$$dn=dz \quad z^2 \exp(-z/1.5) \quad (23)$$

with reaching higher limiting magnitudes and having relatively accurate photometric redshifts [39].

The cosmological parameters considered in this paper are  $(A_0; n_s; s; \Omega_m; \Omega_b; Y_H; s; z_{\text{re}}; m)$  and  $(r_1, \dots, r_8; F_1, \dots, F_8)$ . The Fisher matrix analysis is used to estimate the constraints on all 25 cosmological parameters simultaneously. We show the constraints on  $r_i$  and  $F_i$  in the following subsections.

#### A. Constraints on the angular diameter distance

The extensive window function defined by  $W(r; r)$   $T(k)$  is bell-shaped. As  $r$  is close to  $r_i$ , the extensive window function decreases due to the numerator term of  $W$  in Eq. 18. And as  $r$  is close to zero, the extensive window function also decreases since the transfer function decreases at high  $k = l=r$ . The variation of  $r_i$  contributes to shift the peak point of the extensive window function. Larger median distance leads to more contribution of the smaller  $k$  modes to cosmic shear correlation functions.

As is shown in Fig. 2, the angular diameter distance evolution is well-reconstructed by tomographic cosmic shear. The mean angular diameter distances  $r_i$  are directly measured in high accuracy around a few percentage level.

#### B. Constraints on the growth factor

The variation of  $F_i$  has no impact on the shear correlations in bin  $j$  less than  $i$ . The response to the variations of  $F_i$  in bin  $j = 1$  is a unique signature of a parameter  $F_1$ . Such a ladder structure helps to break degeneracy among the eight  $F_i$  parameters. The constraints on  $F_i$  at higher redshift bin are weakened since fewer shear correlation power spectra are influenced by  $F_i$ .

Based upon the measurement of the primordial scalar amplitude  $A_0$  at the last scattering surface,  $(\ln A_0) \pm 0.17$ , we proceed to construct the growth factor from higher redshift bins. The growth factor history is precisely reconstructed up to  $z = 2$  with the ground-based surveys and up to  $z = 1.2$  with the space-based surveys as shown in Fig. 3.

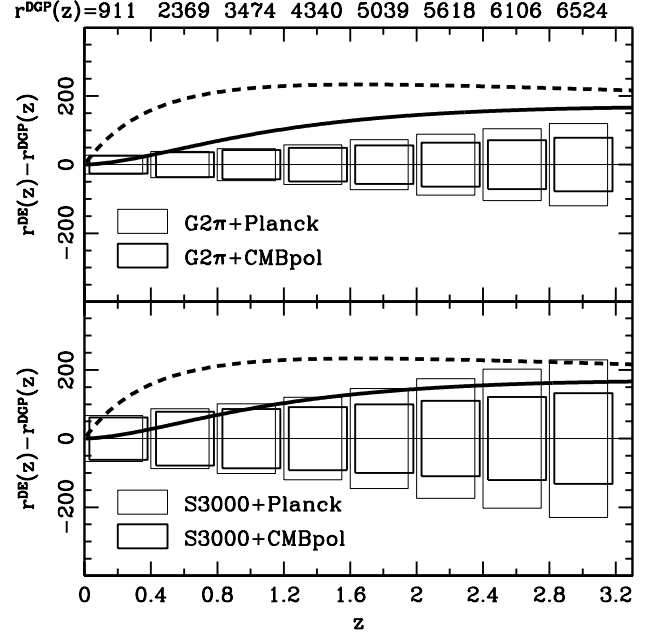


FIG. 2: Constraints on the direct measurement of the angular diameter distance: The error boxes are the level of accuracy to determine  $r_i$  in each bin. The solid curves represent the  $r_i$  of ModelDEr and the dash curves represent the  $r_i$  of ModelDEF.

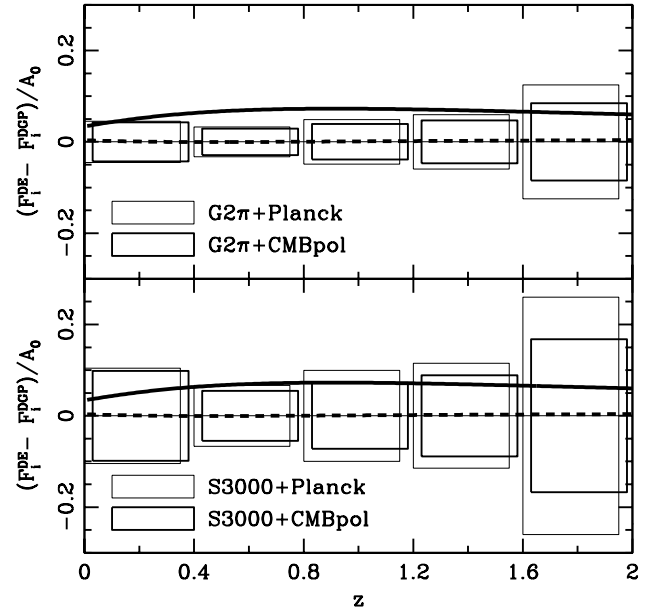


FIG. 3: Constraints on the direct measurement of the growth factor: The error boxes are the level of accuracy to determine  $F_i$  as defined in Eq. 20. The solid curves represent the  $F_i$  of ModelDEr and the dash curves represent the  $F_i$  of ModelDEF.

# V. CAN WE DISCRIMINATE DGP FROM DE?

The direct measurements of the eight  $r_i$  parameters and the eight  $F_i$  parameters allow us to find the parameters that fit  $r_i$  and  $F_i$ . In the DGP model, the  $r_i$  and  $F_i$  are completely fixed by 9 other parameters ( $A_0; n_S; s; i_m; i_b; Y_{He}; s; z_{re}; m$ ) and the flatness constraint. We assume that the fixed  $r_i$  and  $F_i$  of DGP are fiducial values. In the DE model, the  $r_i$  and  $F_i$  are still variable by the equation of state of dark energy  $w$  (a) even with all constraints given by 9 other parameters and the flatness. We parameterize  $w$  (a) as  $w = w_a(1 - a)$  [9] and vary  $(w; w_a)$  of DE to fit the fiducial  $r_i$  and  $F_i$ . Model DER denotes the best DE model to fit the fiducial  $r_i$  and Model DEF denotes the best DE model to fit the fiducial  $F_i$ . In Fig. 2 and Fig. 3, Model DER and Model DEF provide the solid curves and the dash curves respectively.

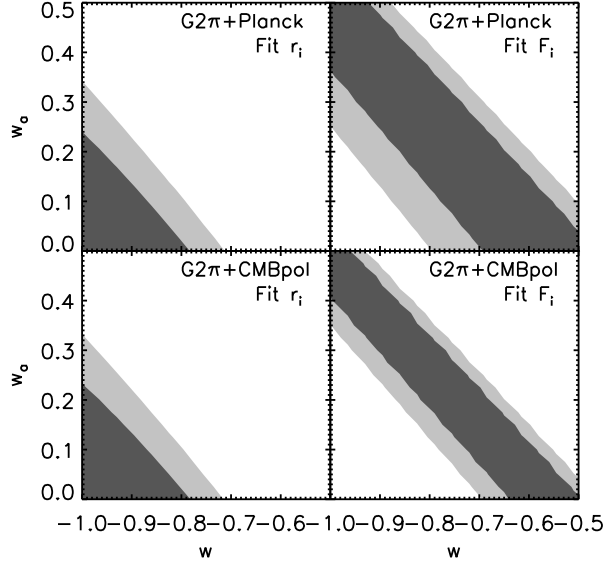


FIG. 4: Contourplots showing constraints on the DE parameters with G2, assuming the true model DGP. The contours in left panels cover DE parameter space to fit  $r_i$  and the contours in right panels cover DE parameter space to fit  $F_i$ . The fiducial model is the DGP model and we vary DE parameters  $(w; w_a)$  to fit the  $r_i$  and  $F_i$ . The inner curves represent 1- confidence level and the outer curves represent 2- confidence level.

While the  $F_i$  of Model DEF is nearly identical with the fiducial  $F_i$ , the  $r_i$  of Model DER is distinct from the fiducial  $r_i$ . The angular diameter distance to the last scattering surface at  $z = 1100$  is almost fixed by the prior information of  $s$  and  $i_m$ . When we fix the angular diameter distance at  $z = 1100$ , we do not find any DE model which generates  $r_i$  nearly identical with the fiducial  $r_i$  by varying  $(w; w_a)$ . By fitting  $r_i$ , DGP is able to be discriminated from DE models parameterized with

$(w; w_a)$ . However, any one of DE and DGP models is not excluded more than 90% confidence level with fitting  $r_i$  alone. Also considering the generic aspect of DE, we can differently parameterize  $w$  (a) to fit better the fiducial  $r_i$ . Thus it is not clear yet to discriminate DGP from DE by fitting  $r_i$  alone unless DGP is excluded by its poor fit to  $r_i$ .

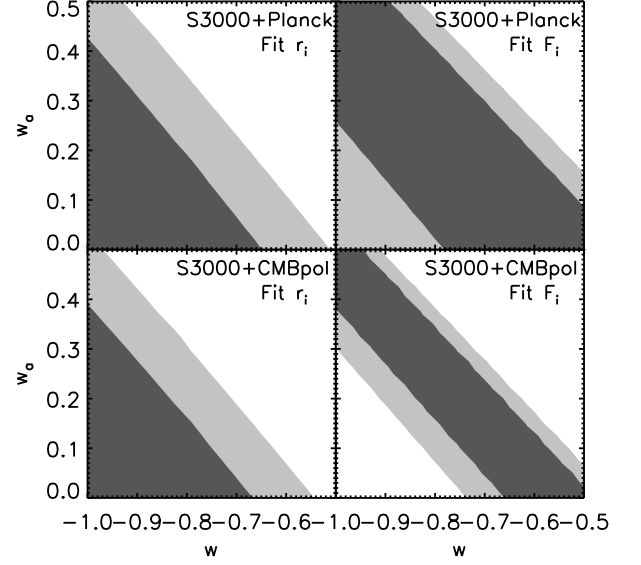


FIG. 5: Contourplots showing constraints on the DE parameters with S3000, assuming the true model DGP. The contours in left panels cover DE parameter space to fit  $r_i$  and the contours in right panels cover DE parameter space to fit  $F_i$ . The fiducial model is the DGP model and we vary DE parameters  $(w; w_a)$  to fit the  $r_i$  and  $F_i$ . The inner curves represent 1- confidence level and the outer curves represent 2- confidence level.

Next we consider fitting the  $r_i$  and  $F_i$  simultaneously. Despite a good fit with the fiducial  $F_i$ , Model DEF is excluded by a poor fit with the fiducial  $r_i$ . The distinct suppression in the DGP growth factor leads to the separation in two regions of the DE parameter space to fit the  $r_i$  and the  $F_i$ . In Fig. 4 and Fig. 5, we show the disagreement between two DE parameter spaces in detail. The ground-based cosmic shear survey G2 clearly discriminates DGP from DE around 95% confidence level (Fig. 4). And the space-based cosmic shear survey S3000 is able to see the difference between DE and DGP around 68% confidence level (Fig. 5). Although the space-based surveys in our analysis do somewhat worse because of the smaller sky coverage, we must remind the reader that we are focusing on science that can be done with information on the larger angular scales. Space-based observations will have advantages with respect to ground-based observations at smaller angular scales.

In conclusion, DGP is distinguishable from DE by a

cosmic shear survey. The DGP model is not yet clearly ruled out by any experiment. For instance, it is too early for us to rule out DGP by using  $\delta_8$  at this moment. As shown in Fig. 3, the normalization induced by DGP could be around 5% less. However considering the current constraints on the primordial amplitude  $A_0$  (more than 5% uncertainty), we are not able to discriminate DGP from DE by  $\delta_8$  alone with current datasets. We still have a chance to detect the extra dimension in the future.

The DGP growth factor predicted by [20] excluded the DGP model by more suppression than ours. Lue et. al. [20] derived the gravitational perturbations of spherically symmetric clustered matter sources on the cosmological background. However the current solution is possibly missing the significant contribution of quadrature contribution (private communication with Román Scoccimarro).

marro) and we are not able to compare both different methods at this moment.

In case the future cosmic shear surveys prefer DGP to DE, then we will also be able to precisely determine the crossover length scale  $r_c$ . The knowledge of  $r_c$  will lead to the discovery of a fundamental energy scale and mark the beginning of experimental exploration of extra dimensions.

**Acknowledgments :** This work is supervised by Lloyd Knox as a partial fulfillment of PhD dissertation. We appreciate helpful comments from Nemanja Kaloper, Manoj Kaplinghat, Jin-Young Kim, Arthur Lue, Román Scoccimarro and Lorenzo Sorbo. This material is based upon work supported by the National Science Foundation under Grant No. 0307961 and U.S. Dept. of Energy contract DE-FG 02-90ER-40560.

- 
- [1] A.G. Riess, A.V. Filippenko, P. Challis, A.C. Iocchiatti, A.D. Jerks, P.M. G. Amavich, R.L.G. Gilliland, C.J. Hogan, S. Jha, R.P. Kirshner, et al., *Astron. J.* 116, 1009 (1998).
  - [2] S. Perlmutter et al. (Supernova Cosmology Project), *Astrophys. J.* 517, 565 (1999), [astro-ph/9812133](#).
  - [3] S. Perlmutter, M.S. Tumer, and M. White, *Phys. Rev. Lett.* 83, 670 (1999).
  - [4] B. Ratra and P.J.E. Peebles, *Phys. Rev. D* 37, 3406 (1988).
  - [5] L.-M. Wang, R.R. Caldwell, J.P. Ostriker, and P.J. Steinhardt, *Astrophys. J.* 530, 17 (2000), [astro-ph/9901388](#).
  - [6] G.R. Dvali, G. Gabadadze, and M. Porrati, *Phys. Lett. B* 485, 208 (2000), [hep-th/0005016](#).
  - [7] S.M. Carroll, *Living Rev. Rel.* 4, 1 (2001), [astro-ph/0004075](#).
  - [8] J. Weller and A. Albrecht, *Phys. Rev. Lett.* 86, 1939 (2001), [astro-ph/0008314](#).
  - [9] E.V. Linder (2002), [astro-ph/0210217](#).
  - [10] D. Huterer and G. Starkman, *Phys. Rev. Lett.* 90, 031301 (2003), [astro-ph/0207517](#).
  - [11] J. Weller and A.M. Lewis, *Mon. Not. Roy. Astron. Soc.* 346, 987 (2003), [astro-ph/0307104](#).
  - [12] R. Bean and O. Dore, *Phys. Rev. D* 69, 083503 (2004), [astro-ph/0307100](#).
  - [13] Y.-S. Song and L. Knox (2003), [astro-ph/0312175](#).
  - [14] J. Kratochvil, A. Linde, E.V. Linder, and M. Shmalkova (2004), [astro-ph/0312183](#).
  - [15] C. De Ayet, *Phys. Lett. B* 502, 199 (2001), [hep-th/0010186](#).
  - [16] C. De Ayet, G.R. Dvali, and G. Gabadadze, *Phys. Rev. D* 65, 044023 (2002), [astro-ph/0105068](#).
  - [17] N. Arkani-Hamed, S. Dimopoulos, and G.R. Dvali, *Phys. Lett. B* 429, 263 (1998), [hep-ph/9803315](#).
  - [18] L. Randall and R. Sundrum, *Phys. Rev. Lett.* 83, 3370 (1999), [hep-ph/9905221](#).
  - [19] L. Randall and R. Sundrum, *Phys. Rev. Lett.* 83, 4690 (1999), [hep-th/9906064](#).
  - [20] A. Lue, R. Scoccimarro, and G.D. Starkman, *Phys. Rev. D* 69, 124015 (2004), [astro-ph/0401515](#).
  - [21] W. Hu, *Astrophys. J.* 522, L21 (1999), [astro-ph/9904153](#).
  - [22] W. Hu, *Phys. Rev. D* 65, 23003 (2002).
  - [23] B. Jain and A. Taylor, *Phys. Rev. Lett.* 91, 141302 (2003), [astro-ph/0306046](#).
  - [24] G.M. Bernstein and B. Jain, *Astrophys. J.* 600, 17 (2004), [astro-ph/0309332](#).
  - [25] M. Takada and B. Jain, *Mon. Not. Roy. Astron. Soc.* 344, 857 (2003), [astro-ph/0304034](#).
  - [26] J. Zhang, L. Hui, and A. Stebbins (2003), [astro-ph/0312348](#).
  - [27] P.P. Avelino and C.J.A.P. Martins, *Astrophys. J.* 565, 661 (2002), [astro-ph/0106274](#).
  - [28] C. De Ayet, S. J. Landau, J. Raux, M. Zaldarriaga, and P. A. Stier, *Phys. Rev. D* 66, 024019 (2002), [astro-ph/0201164](#).
  - [29] G. Dvali and M.S. Tumer (2003), [astro-ph/0301510](#).
  - [30] A.G. Riess et al. (Supernova Search Team) (2004), [astro-ph/0402512](#).
  - [31] S. Mukohyama, *Phys. Rev. D* 62, 084015 (2000), [hep-th/0004067](#).
  - [32] C. De Ayet, *Phys. Rev. D* 66, 103504 (2002), [hep-th/0205084](#).
  - [33] N. Kaiser, *Astrophys. J.* 388, 272 (1992).
  - [34] M. Bartelmann and P. Schneider, *Phys. Rep.* 340, 291 (2001), [astro-ph/9912508](#).
  - [35] M. Kaplinghat, L. Knox, and Y.-S. Song, *Phys. Rev. Lett.* 91, 241301 (2003), [astro-ph/0303344](#).
  - [36] M. Kaplinghat et al., *Astrophys. J.* 583, 24 (2003), [astro-ph/0207591](#).
  - [37] M. Nagashima, Y. Yoshii, T. Totani, and N. Gouda, *Astrophys. J.* 578, 675 (2002), [astro-ph/0207483](#).
  - [38] J.A. Tyson, D.M. Wittman, J.F. Hennawi, and D.N. Spergel, *Nucl. Phys. Proc. Suppl.* 124, 21 (2003), [astro-ph/0209632](#).
  - [39] R. Massey et al. (2003), [astro-ph/0304418](#).